Catal Lett (2011) 141:198–206
DOI 10.1007/s10562-010-0470-5

The Catalytic Use of Supported Gold Nanoparticles for Styrene Synthesis Via Oxidative Dehydrogenation of Ethylbenzene

Jie Xu · Jun Huang · Yong-Mei Liu · Yong Cao · Yong-Xin Li · Kang-Nian Fan

Received: 16 August 2010 / Accepted: 8 October 2010 / Published online: 26 October 2010

Abstract A series of supported gold catalysts have been prepared and tested as a new type of catalyst for the oxidative dehydrogenation of ethylbenzene to styrene. The effects of the supports (α-Mn_2O_3, Fe_2O_3, TiO_2, Al_2O_3, and CeO_2), preparation methods, gold loadings, and reaction conditions have been investigated. Among the catalysts tested, the Au/CeO_2 sample containing a 6.0 wt% gold content prepared via a routine deposition–precipitation method exhibited the highest ethylbenzene conversion (66.9%) and remarkable styrene selectivity (91.0%). The superior catalytic performance of the Au/CeO_2 catalysts can be attributed to a dramatic increase in the oxygen mobility and storage capacity of the parent CeO_2 material in association with the closely contacted Au nanoparticles, which is confirmed by the TPR, total OSC, and XPS measurements.

Keywords Gold · Ceria · Oxidative dehydrogenation (ODH) · Ethylbenzene

Electronic supplementary material The online version of this article (doi:10.1007/s10562-010-0470-5) contains supplementary material, which is available to authorized users.

J. Xu · Y.-X. Li (✉)
College of Chemistry and Chemical Engineering, Changzhou University, Gehu Road 1, Changzhou, Jiangsu 213164, People's Republic of China
e-mail: liyx@em.jpu.edu.cn

J. Huang · Y.-M. Liu · Y. Cao · K.-N. Fan
Shanghai Key Laboratory of Molecular Catalysis and Innovative Materials, Department of Chemistry, Fudan University, Shanghai 200433, People's Republic of China

1 Introduction

In the past decade, catalysis by gold has emerged as one of the most intensively studied topics in chemistry. Au was historically considered to be chemically inert and hence a poor catalyst [1, 2]. However, when finely divided as small particles (≤5 nm) and suitably deposited onto an oxide support [3, 4], Au could become a highly active and selective catalyst in many reactions including oxidation [5–7], hydrogenation [8], selective isomerization [9] and one-pot multistep reactions [10–12]. The outstanding catalytic ability of Au is related to the size and shape of the nanoparticles (NPs), the degree of coordinative unsaturation of the Au atoms, and the interactions between Au and the oxide support [2–4]. Of particular interest to the current chemical community is the Au-catalyzed selective oxidation, which is believed to be essential for the development of new alternative and greener routes toward sustainability [7, 13]. One recent focus in this area is to expand the scope of the selective aerobic oxidations [5–7] that can be efficiently catalyzed by supported Au NPs. In this context, several liquid phase aerobic oxidations, including the selective oxidation of alcohols [13–16], aldehydes [17], amines [12, 18, 19], oximes [20] and olefinic hydrocarbons [7, 13] have been developed. Despite significant research effort, there have been few studies on the selective oxidation of less reactive hydrocarbons in the gas phase over the supported Au NPs [21, 22], probably due to the fact that both the reactants and products are prone to undesired combustion in the presence of molecular oxygen at high temperatures [23–25].

Styrene (ST) is one of the most important monomers extensively used in the chemical industry for the manufacture of polymers, copolymers and reinforced plastics [26]. In 2009, the worldwide production of ST was more

than 23 megatons (http://www.sriconsulting.com/WP/Public/Reports/styrene/). Most of the ST monomer is commercially produced by means of the direct catalytic dehydrogenation (DH) of ethylbenzene (EB) at high reaction temperatures (600–650 °C), with multi-promoted potassium-iron oxide as a catalyst [27, 28]. Due to its highly endothermic nature, this traditional route suffers from several pronounced disadvantages such as intensive energy consumption and rapid coking. In the last few years, considerable research efforts have been directed toward the development of less energy-intensive processes for the production of ST [26]. The catalytic oxidative dehydrogenation (ODH) of EB in the presence of air or molecular oxygen (O_2) is an attractive alternative to the traditional DH process [29–31], which is thermodynamically favored at much lower temperatures and usually does not lead to the formation of coke. However, this selective oxidation is particularly challenging, given the high reactivity of ST toward further oxidation.

To date, the most promising catalysts suggested for this process have been confined to several carbon nanostructures including onion like carbon (OLC) [30, 32] or carbon nanofibers (CNF) [33, 34]. Nevertheless, the fine powdered nature, and intrinsically low resistance to combustion of the carbon-based nanomaterials have greatly hindered their practical applications [35]. Very recently, we have reported that high surface area (180 $m^2\ g^{-1}$) mesostructured ceria material featuring superior low temperature redox properties can catalyze the ODH of EB at temperatures around 450 °C [36]. In the present work, we report the development of new efficient ceria supported gold catalyst system exhibiting significantly enhanced activity and stability for the ODH of EB. Our results have shown that the introduction of gold nanoparticles can lead to a dramatic increase in the oxygen mobility and oxygen storage capacity of the parent CeO_2 material, which makes the catalysts highly active and stable for the reaction.

2 Experimental

2.1 Catalyst Preparation

A series of Au/CeO_2 catalysts were prepared via a routine deposition–precipitation (DP) method with NaOH as the precipitation agent [1]. Briefly, 1 g CeO_2 (Evonic, Adnano 90, surface area: 90 $m^2\ g^{-1}$) was added to an aqueous solution with desired amount of $HAuCl_4$ and NaOH (NaOH/Au = 100, molar ratio). The suspension was then heated to 80 °C and stirred for 4 h, followed by filtering and washing for several times with distilled water. The resulting solid product was dried overnight and finally a purple colored catalyst was obtained by reduction of the DP-derived materials at 450 °C for 4 h in 5 vol%H_2/Ar gas. The final catalyst is denoted as *n*Au/CeO_2-DP hereinafter where DP denotes the routine NaOH-mediated DP method, *n* represents the nominal Au loading.

To investigate the effect of preparation method on Au ODH activity, two additional 4 wt% Au/CeO_2 samples were prepared by urea-mediated deposition–precipitation (UDP) and conventional wet impregnation (IMP) methods. In addition, a Au/α-Mn_2O_3 catalyst was prepared, as Au/α-Mn_2O_3 catalysts had been reported to show good low temperature CO activity [37]. Au was deposited to the α-Mn_2O_3 support by the UDP method. A further series of gold catalysts including Au/TiO_2 (Type A, Lot no. Au/TiO_2 #02-1), and Au/Fe_2O_3 (Type C, Lot no. Au/Fe_2O_3 #02-5) were supplied by the World Gold Council, Au/Al_2O_3 (catalogue no. 79-0160) was provided by Mintek.

2.2 Characterization of Catalysts

Structural analysis of the various Au/CeO_2 catalysts was carried out on a Bruker D8 Advance X-ray diffractometer equipped with a graphite monochromator, operating at 40 kV and 40 mA and employing nickel-filtered Cu-Kα radiation ($\lambda = 1.5406$ Å). The morphologies of all Au/CeO_2 catalysts were studied by JEOL 2010 electron microscope. The bulk loading amount of Au in all Au/CeO_2 catalysts were measured by inductively coupled plasma atomic emission spectroscopy (ICP-AES). Temperature programmed reduction (TPR) profiles were obtained on a homemade apparatus. The samples were pretreated in a mixed gas ($O_2/N_2 = 1/8$) at 450 °C for 30 min and cooled to room temperature. Subsequently, the samples were reduced with 5 vol% H_2/Ar at 40 mL min^{-1} with a ramping rate of 5 °C min^{-1} to ca. 900 °C. The H_2 consumption was monitored by an on-line thermal conductivity detector (TCD). X-ray photoelectron spectra (XPS) analysis was performed on a Perkin Elmer PHI 5000C spectrometer using Mg Kα radiation (1253.6 eV, pass energy of 20.0 eV). The carbonaceous C 1s line (284.6 eV) was used as the reference to calibrate the binding energies (BE).

2.3 Catalytic Activity Measurements

The activity of the catalysts for ODH of EB was measured in the temperature range of 350–500 °C at atmospheric pressure using a fix-bed, down-flow, tubular quartz reactor (i.d. 4 mm, length 400 mm). Each run used approximately 50 mg of catalyst in the form of 60–80-mesh particles, mixed with 300 mg of silicon carbide grains of similar size for best temperature control. EB was evaporated at 35 °C in flowing N_2 and subsequently mixed with O_2. Unless otherwise stated, the corresponding flow rate of EB, O_2,

and N_2 is fixed at 0.5, 0.25 and 20 mL min^{-1} (GHSV = 19,972 h^{-1}), respectively. Prior to testing, the catalysts were pretreated in a mixed gas (O_2/N_2 = 1/8) at 450 °C for 30 min. The products were analyzed by an on-line gas chromatograph (Agilent GC 6820). Permanent gases (O_2, CO, CO_2) were separated using a TDX-01 column connected to a TCD detector and other reaction products were analyzed employing a FFAP column connected to a FID detector. The catalytic data were acquired after 1 h on stream of the reaction. The carbon balance closed to 100 ± 5% and was additionally monitored by the CO_x content after catalytic combustion of organic species in a final total oxidation reactor.

2.4 Total OSC Measurement

The total oxygen storage capacity (OSC) measurement was tested at 450 °C. 25 mg ceria-supported Au catalyst diluted with 300 mg silicon carbide grains of similar size was placed in a quartz U-shape reactor. The concentration of the three components (H_2, H_2O, and He) in the outlet gas was monitored by an on-line mass spectrometer (Balzers OmniStar, QMS 200). A sample was exposed to alternating H_2 (40 mL min^{-1} for 10 s) and He (40 mL min^{-1} for 80 s) pulses, and the alternating pulsation lasted until the signal intensity of H_2 reached a balance (100 ± 5%). Total OSC was calculated by integrating the consumption of H_2 [μmol [O] g^{-1}].

3 Results and Discussion

3.1 Catalytic Tests

Initially, a range of Au catalysts supported on various inorganic supports were applied to the ODH of EB under a previously established reaction condition at 450 °C [36]. As can be seen from Table 1, the chemical nature of the support has a strong influence on the catalytic performance of the Au NPs. Of the various Au-based catalysts tested, 2.0Au/CeO_2-DP (Table 1, entry 5) prepared by the routine DP method showed the highest activity in terms of the selective formation of ST. The steady-state ST selectivity obtained was as high as 90.0% which indicated the success in depressing secondary oxidation, in sharp contrast to what was observed for most of the other supported Au catalysts (Table 1, entries 1–4). A clear advantage of the Au/CeO_2-DP catalyst over other noble metals was also noticed when the reaction was performed using Pt/CeO_2 or Ru/CeO_2 under otherwise identical conditions (Table 1, entries 6, 7). It is important to remark that in the presence of small amount of O_2 (n_{O2}/n_{EB} = 0.5), the performances of Au/CeO_2 were comparable to or even higher than those of the typical iron catalysts (Supporting Information, Table S1), noting that we did not introduce any steam in the ODH tests. However, for the commercial DH process, steam (with high steam/oil ratio (S/O)) as an inert diluent is always required to provide heat, to regenerate the iron-based active sites from coking and to shift the equilibrium conversion of EB, which results in large energy consumption.

Further detailed studies were carried out using the 2.0Au/CeO_2-DP catalyst to gain insights into the catalytic requirements for the ODH of EB. First, the effect of the reaction temperature was investigated and is illustrated in Fig. 1. The EB conversion increased rapidly as the reaction temperature was raised from 350 to 450 °C but leveled off at 500 °C, with the selectivity of ST decreases gradually from ca. 97% to 85%. In all cases, ST was obtained as the major product, accompanied by appreciable amounts of CO_x and very small amount of other byproducts such as benzaldehyde or methyl benzyl alcohol. Presumably, higher temperature should give rise to better catalytic activity for the ODH reaction. However, as is well known in the literature [2], higher reaction temperature (well above the Tammann temperature of bulk gold, see below) may also lead to the sintering or growth of Au NPs, which can greatly compromised the performance of 2.0Au/CeO_2-DP under these conditions. Moreover, studies on the effect of the oxygen concentration revealed that the stoichiometric O_2/EB ratio (n_{O2}/n_{EB} = 0.5) was the ratio of choice

Table 1 Catalytic performance of various catalysts for ODH of EB

Entry	Catalysts	Au loading (wt%)	Conv. (%)	Selec. (%)	Yield (%)
1	Au/α-Mn_2O_3	2.0	7.9	12.6	1.0
2	Au/Fe_2O_3	4.5	10.1	40.8	4.1
3	Au/TiO_2	1.5	15.2	59.1	9.0
4	Au/Al_2O_3	1.5	12.1	44.3	5.4
5	2.0Au/CeO_2-DP	2.0	32.7	90.0	29.4
6	Pt/CeO_2[a]	2.0	8.4	17.5	1.5
7	Ru/CeO_2[a]	2.0	9.5	24.2	2.3

[a] Pt/CeO_2, Ru/CeO_2 prepared by wet impregnation (IMP), see supporting information for the detailed preparation methods

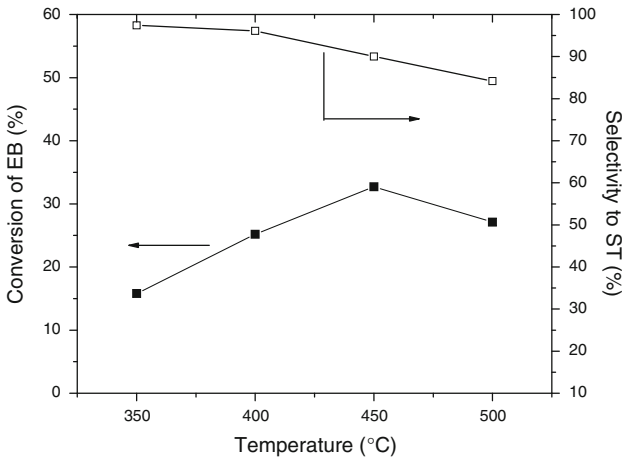

Fig. 1 Catalytic behavior of the 2.0Au/CeO_2 at different reaction temperatures

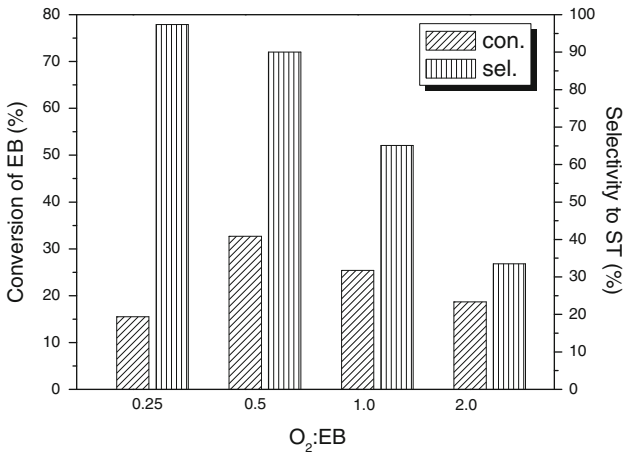

Fig. 2 Effect of molar ratio of O_2 to EB on the catalytic ODH performance of the 2.0 Au/CeO_2-DP catalyst

(Fig. 2). It was clarified that both lower and higher O_2/EB ratios would lead to a great reduction in the reaction rate for the selective formation of ST.

To gain further insights into the function of Au, we have investigated the effect of Au loading on the catalytic performance. As shown in Table 2, EB could only be poorly converted over the parent ceria support [36], whereas the introduction of Au remarkably enhanced EB conversion and selectivity for the partial oxidation products. High selectivity to ST was obtained over the Au/CeO_2 catalysts with higher Au content (Table 2, entries 2–4) and the ST formation increased with the gold loading up to 6.0 wt% Au. However, an even higher Au loading amount with 8.0 wt% would compromise the catalytic activity. As will be discussed later, the undesired formation of larger Au particles (>5 nm) may account for such activity deterioration. The best performance was observed for the catalyst containing 6.0 wt% Au (Table 2, entry 4), which was characterized by high selectivity comparable to the best yet reported for EB ODH [29, 34, 38]. Moreover, in a comparison of three different preparation methods (Table 2, entries 3, 6, 7), it is observed that the Au/CeO_2 catalyst prepared by DP method is more effective. The evolution of the catalytic performance at 450 °C as a function of reaction time for the Au/CeO_2-DP catalysts is shown in Fig. 3. Remarkably, the 6.0 wt% Au/CeO_2 was found to be stable during the reaction, and the ST yield did not undergo appreciable changes with the time on stream.

3.2 Catalyst Characterization

The ICP-AES analysis (Table 2) shows that the real amount of gold deposited on CeO_2 is ca. 10–25% lower than the nominal Au loading, consistent with the known fact that only limited amount of gold contained in the solution can be deposited onto an oxide support via the routine DP method [3]. The specific surface areas for the various Au/CeO_2-DP catalysts were similar to those for the parent support (Table 2). The XRD pattern of the parent ceria (Fig. 4) show well-defined diffraction feature characteristics of the cubic fluorite structure of CeO_2 (JCPDS card no. 34-0394). After the deposition of Au NPs onto the ceria support, an almost identical XRD pattern

Table 2 Catalytic performance of the Au/CeO_2 catalysts for ODH of EB

Entry	Catalysts	Actual Au loading (wt%)	Surface area (m^2 g)	Conv. (%)	Selec. (%)			Yield (%)
					ST	CO_x	Others[a]	
1	CeO_2	–	88	19.5	80.2	17.2	2.6	15.6
2	2.0Au/CeO_2-DP	1.5	78	32.7	90.0	6.6	3.4	29.4
3	4.0Au/CeO_2-DP	2.8	75	50.6	92.4	3.7	3.9	46.8
4	6.0Au/CeO_2-DP	4.0	70	66.9	91.0	0.3	8.7	60.9
5	8.0Au/CeO_2-DP	6.2	68	65.4	88.1	3.4	8.5	57.6
6	4.0Au/CeO_2-IMP	3.8	65	40.2	57.2	10.4	32.4	23.0
7	4.0Au/CeO_2-UDP	3.2	70	47.0	57.4	8.5	34.1	26.9

[a] Benzene, benzaldehyde, and methylbenzyl alcohol based on GC analysis

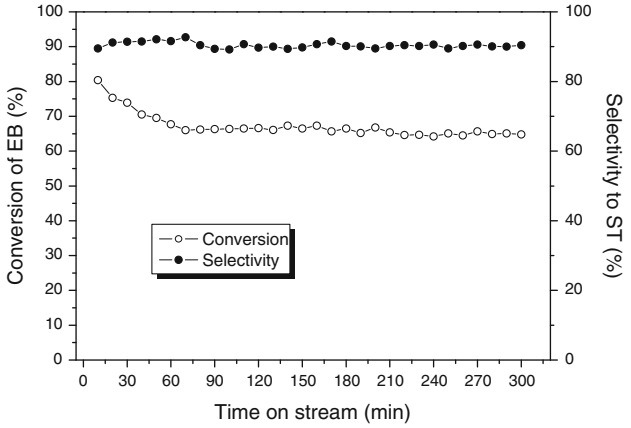

Fig. 3 Time on stream of EB ODH on 6.0Au/CeO_2-DP

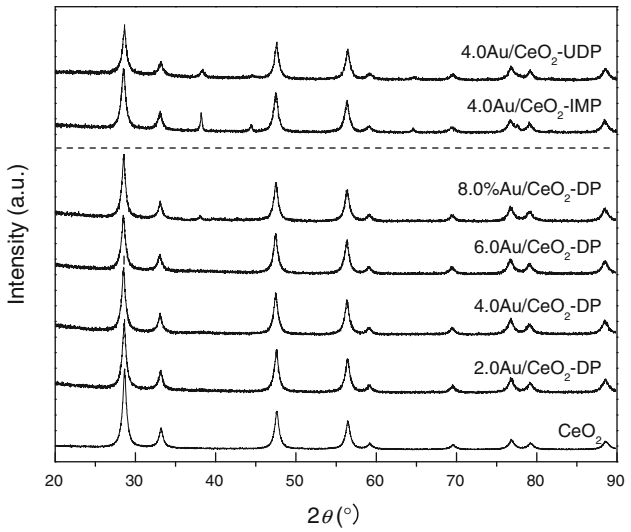

Fig. 4 XRD patterns of Au/CeO_2-DP, 4.0Au/CeO_2-IMP and 4.0Au/CeO_2-UDP samples

was obtained for Au/CeO_2-DP comparing with CeO_2, indicating that the crystalline structure and the average size of the crystalline domain of the CeO_2 support are well maintained in the gold samples. Moreover, no peaks due to gold species were detected, except in the case of the 8.0Au/CeO_2-DP sample, where a distinct metallic Au reflection line at $2\theta = 38.2°$ appears. Figure 4 also compared the effect of the preparation methods on the size of the Au NPs. It is revealed that the UDP- and IMP-derived 4.0Au/CeO_2 catalysts already show distinct metallic Au diffraction lines, in sharp contrast to the absence of any Au features as observed for the 4.0Au/CeO_2-DP sample with a similar gold content. The average gold crystalline size, calculated by Scherrer equation, was 5.3, 6.2 and 10.3 nm for the 8.0Au/CeO_2-DP, 4.0 Au/CeO_2-UDP and 4.0Au/CeO_2-IMP samples, respectively.

TEM was used as a complementary technique to examine the structures of gold particles. Representative TEM images for the various catalysts are shown in Fig. 5. In the case of the Au/CeO_2-DP samples, the Au NPs were small and evenly dispersed over the 2.0Au/CeO_2-DP with an average particle size of ca. 3.6 nm. With increasing gold loading, a progressive increase in the Au particle size can be observed. A considerable fraction of Au particles with particle size larger than 5.0 nm was detected over the catalyst containing 8.0 wt% Au. The TEM analysis of the 4.0Au/CeO_2-IMP as well as 4.0Au/CeO_2-UDP also showed the presence of appreciable fraction of Au particles larger than 5 nm over the support, in good agreement with the XRD data as described above. All these results strongly suggest that the NaOH DP method is more suitable to achieve a high dispersion of Au NPs with small Au particle size (<5 nm) over the ceria support. Additionally, it is interesting to point out that after 5 h on stream of the reaction at 450 °C, the size of Au NPs has not undergone noticeable changes, which could partly explain the stability of the catalyst. We note that this lack of agglomeration indicates that, when properly prepared and in association with a suitable support, supported gold NPs can serve as a stable catalyst for high temperature applications, although it is known that gold has a relatively low Tammann temperature (395 °C) [39]. Presumably, the presence of a strong metal-support interaction (SMSI) between the gold particles and the underlying CeO_2 support may play a key role in stabilizing the Au particles [40, 41].

TPR experiments were carried out to gain an insight into the redox properties of the various catalysts. As shown in Fig. 6, two main peaks at low (peak α) and high temperature (peak β) are observed for all samples, assignable to the reduction of surface- capping oxygen and bulk oxygen species, respectively. While the blank ceria showed a broad low temperature reduction profile in the range 250–500 °C, the introduction of Au species drastically decreases the temperature of the peak α. The lowest temperature (ca. 77 °C) was observed over 6.0Au/CeO_2-DP, a feature signifying superior low temperature reducibility. In addition, OSC measurements at 450 °C revealed a limited OSC of ca. 140 μmol [O] g^{-1} over the parent ceria material (Fig. 7). This value is consistent with the broad literature [42–44] showing that the reduction of ceria surface layers is limited to 5.0%. When Au NPs were deposited onto the ceria, the XP spectrum of the Au $4f_{7/2}$ core level shows a predominant contribution from metallic Au^0 at a binding energy of 84.0 eV [45] (Fig. 8). Notably, it was found that the loading of Au caused a significant modification in the oxygen storage behavior of the ceria materials. These results can be rationalized by assuming that the presence of small Au NPs can result in the favorable enhanced oxygen mobility in the surface layers of ceria, mostly due to the

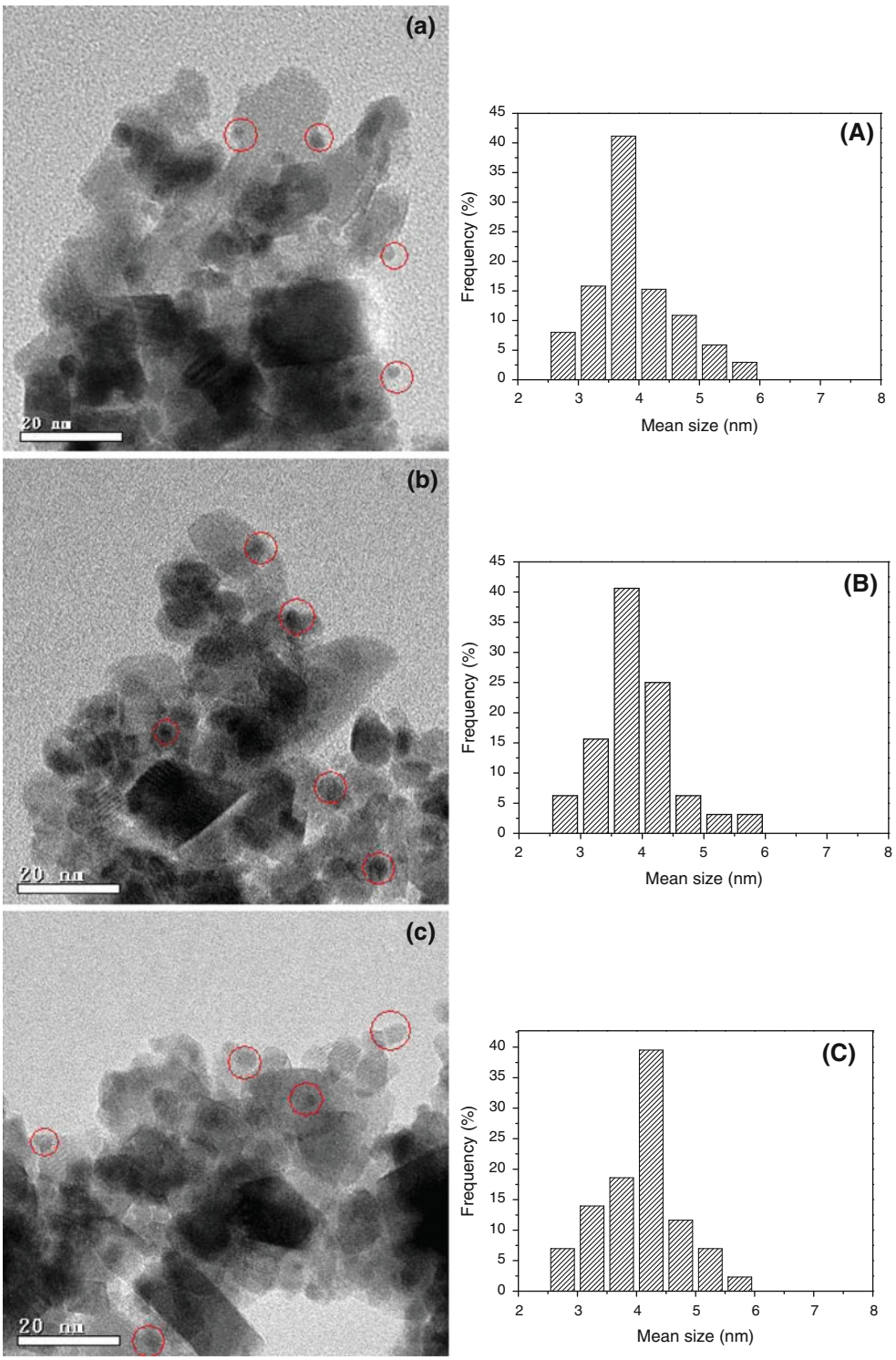

Fig. 5 TEM images of 2.0Au/CeO_2-DP (**a**), 4.0Au/CeO_2-DP (**b**), 6.0Au/CeO_2-DP (**c**), 8.0Au/CeO_2-DP (**d**), 4.0Au/CeO_2-IMP (**e**), 4.0Au/CeO_2-UDP (**f**), and the spent 6.0Au/CeO_2-DP (**g**) samples

creation of a high abundance of oxygen vacancies in ceria lattice, which are responsible for the considerably enhanced reduction degrees as observed for the Au/CeO_2 catalysts.

Bearing in the mind that the catalytic behaviors of ceria-based materials is highly sensitive to the mobility or amount of the lattice oxygen, to gain further insight into the nature of the DP derived Au/CeO_2 catalysts in relation to

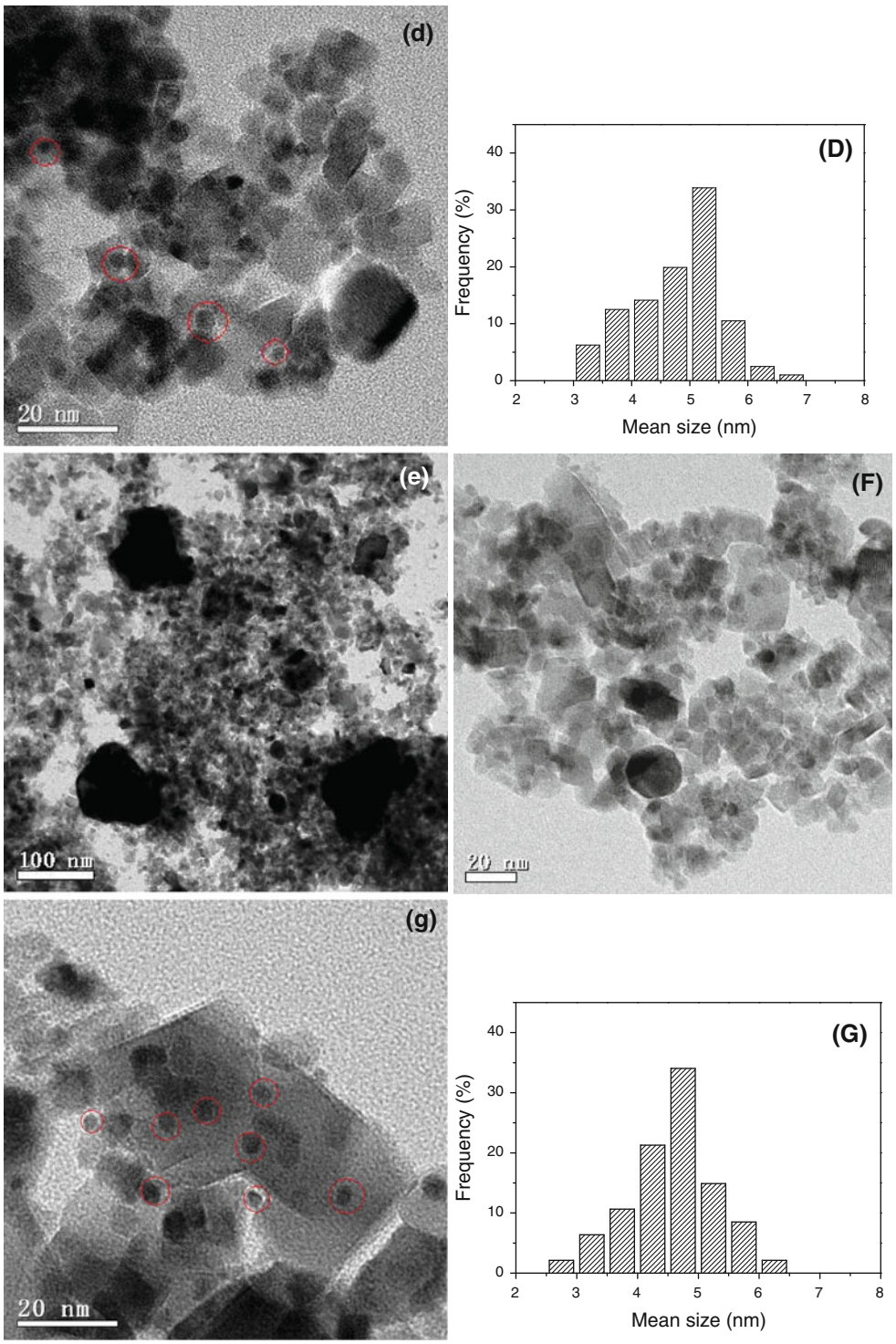

Fig. 5 continued

their ODH activity, the total OSC of the various catalysts are plotted against with the corresponding reaction rate. As shown in Fig. 7, the amount of available lattice oxygen species in the Au/CeO_2 material directly correlates the catalytic activity of CeO_2 in the ODH of EB reaction, permitting a rational explanation for the positive effect of Au loading on the performance of the catalyst. We therefore infer that the present ODH of EB over the Au/CeO_2-based catalysts may proceed via a simple redox mechanism involving the Ce^{4+}/Ce^{3+} couple, in which the catalyst

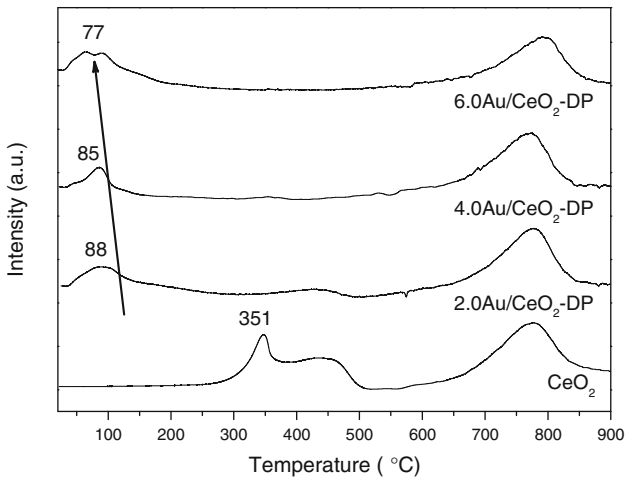

Fig. 6 TPR profiles of the Au/CeO_2-DP and CeO_2 samples

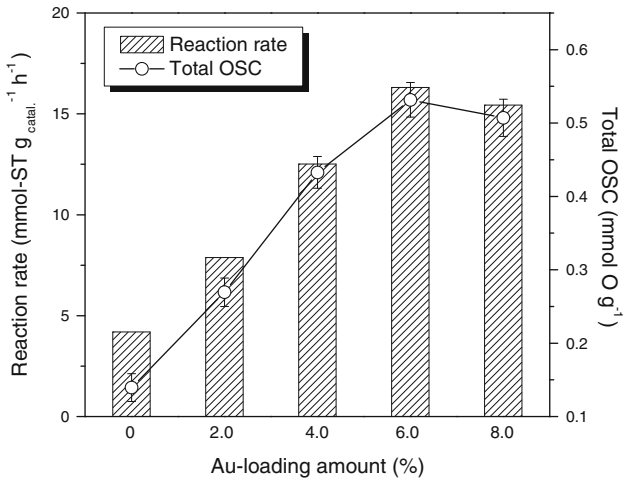

Fig. 7 Correlation between the reaction rates of the Au/CeO_2 catalysts with their corresponding total OSC at 450 °C

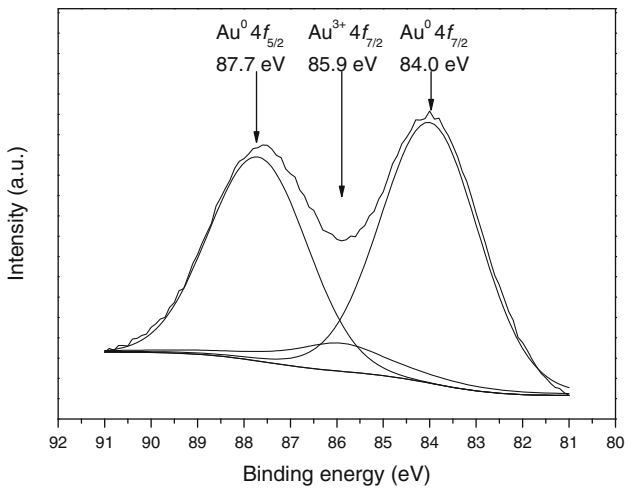

Fig. 8 XP spectrum (Au 4*f*) of the fresh $6.0Au/CeO_2$-DP sample

undergoes reduction (by EB) and reoxidation (by O_2) cycles. In this sense, the overall reaction pathway can be envisaged to involve a delicate redox interplay between Au clusters and the CeO_2 matrix during the EB ODH process, i.e., the reaction proceeds via a facile Au-mediated oxygen-transfer mechanism in which the consumption and replenishment of the ceria lattice surface oxygen species vicinal to Au NPs play a key role in the reaction process. To testify this hypothesis, XPS studies on Au/CeO_2 subjected to sequential EB/O_2 exposures were carried out. The results show that the consumption and replenishment of the lattice oxygen, as reflected by the distinct atmospheric-dependent variation of the ratio of Ce^{4+}/Ce^{3+} (Fig. S1) is essential for this reaction.

4 Conclusions

In summary, a novel Au-decorated ceria catalyst, featured with superior low temperature catalytic performance, has been developed for the oxidative dehydrogenation of ethylbenzene to styrene. Compare to other noble metal-oxide support combinations, the Au/CeO_2-DP catalysts prepared via a routine deposition–precipitation method exhibited a high activity and selectivity toward the reaction. In the presence of small amount of O_2 ($n_{O2}/n_{EB} = 0.5$), a stable styrene yield over 60% can be obtained over the 6.0Au/CeO_2-DP catalyst at temperatures around 450 °C. Based on the TPR profiles and total OSC results, it was clarified that the introduction of Au nanoparticles ($\leq$5 nm) has drastically enhanced the oxygen mobility and storage capacity of the ceria, thus leading to the significant improvement of its catalytic activity. Furthermore, the XPS results implied that the ODH of ethylbenzene over the Au/CeO_2 catalyst may proceed via a simple surface redox mechanism involving the Ce^{4+}/Ce^{3+} couple.

Acknowledgments This work was financially supported by the National Natural Science Foundation of China (20633030, 20721063, 20803012, and 20873026), the National High Technology Research and Development Program of China (2006AA03Z336), and the National Basic Research Program of China (2009CB623506), Science & Technology Commission of Shanghai Municipality (08DZ2270500).

References

1. Bond GC, Louis C, Thompson D (2006) Catalysis by gold. Imperial College Press, London
2. Bond GC, Thompson DT (1999) Catal Rev 41:319–388
3. Haruta M (2002) Cattech 6:102–115
4. Haruta M (2003) Chem Rec 3:75–87
5. Pina CD, Falletta E, Prati L, Rossi M (2008) Chem Soc Rev 37:2077–2095
6. Hashmi ASK, Hutchings GJ (2006) Angew Chem Int Ed Engl 45:7896–7936

7. Hughes MD, Xu YJ, Jenkins P, McMorn P, Landon P, Enache DI, Carley AF, Attard GA, Hutchings GJ, King F (2005) Nature 437:1132–1135
8. Corma A, Serna P (2006) Science 313:332–334
9. Raptis C, Garcia H, Stratakis M (2009) Angew Chem Int Ed Engl 48:3133–3136
10. Su FZ, Ni J, Sun H, Cao Y, He HY, Fan KN (2008) Chem Eur J 14:7131–7135
11. Sun H, Su FZ, Ni J, Cao Y, He HY, Fan KN (2009) Angew Chem Int Ed Engl 48:4390–4393
12. Grirrane A, Corma A, Garcia H (2008) Science 322:1661
13. Della Pina C, Falletta E, Rossi M (2008) J Catal 260:384–386
14. Enache DI, Edwards JK, Landon P, Solsona-Espriu B, Carley AF, Herzing AA, Watanabe M, Kiely CJ, Knight DW, Hutchings GJ (2006) Science 311:362
15. J rgensen B, Egholm Christiansen S, Dahl Thomsen ML, Christensen CH (2007) J Catal 251:332-337
16. Su FZ, Liu YM, Wang LC, Cao Y, He HY, Fan KN (2008) Angew Chem Int Ed Engl 47:334–337
17. Corma A, Domine ME (2005) Chem Commun 2005:4042–4044
18. Klitgaard SK, Egeblad K, Mentzel UV, Popov AG, Jensen T, Taarning E, Nielsen IS, Christensen CH (2008) Green Chem 10:419–423
19. Zhu B, Lazar M, Trewyn BG, Angelici RJ (2008) J Catal 260:1–6
20. Grirrane A, Corma A, Garcia H (2009) J Catal 268:350–355
21. Moreau F, Bond GC (2007) Catal Commun 8:1403–1405
22. Bravo-Suárez JJ, Bando KK, Lu J, Fujitani T, Oyama ST (2008) J Catal 255:114–126
23. Gluhoi AC, Nieuwenhuys BE (2007) Catal Today 119:305–310
24. Solsona BE, Garcia T, Jones C, Taylor SH, Carley AF, Hutchings GJ (2006) Appl Catal A Gen 312:67–76
25. Sinha AK, Suzuki K, Takahara M, Azuma H, Nonaka T, Fukumoto K (2007) Angew Chem Int Ed Engl 46:2891–2894
26. Cavani F, Trifiro F (1995) Appl Catal A Gen 133:219–239
27. Reddy BM, Rao KN, Reddy GK, Khan A, Park SE (2007) J Phys Chem C 111:18751–18758
28. Lee EH (1973) Catal Rev 8:285–305
29. Zhao TJ, Sun WZ, Gu XY, Ronning M, Chen D, Dai YC, Yuan WK, Holmen A (2007) Appl Catal A Gen 323:135–146
30. Su DS, Maksimova NI, Mestl G, Kuznetsov VL, Keller V, Schlögl R, Keller N (2007) Carbon 45:2145–2151
31. Kustrowski P, Segura Y, Chmielarz L, Surman J, Dziembaj R, Cool P, Vansant EF (2006) Catal Today 114:307–313
32. Keller N, Maksimova NI, Roddatis VV, Schur M, Mestl G, Butenko YV, Kuznetsov VL, Schlögl R (2002) Angew Chem Int Ed Engl 41:1885–1888
33. Delgado JJ, Su DS, Rebmann G, Keller N, Gajovic A, Schlögl R (2006) J Catal 244:126–129
34. Li P, Li T, Zhou JH, Sui ZJ, Dai YC, Yuan WK, Chen D (2006) Microporous Mesoporous Mater 95:1–7
35. Rinaldi A, Zhang J, Mizera J, Girgsdies F, Wang N, Hamid SBA, Schlögl R, Su DS (2008) Chem Commun 6528–6530
36. Xu J, Wang LC, Liu YM, Cao Y, He HY, Fan KN (2009) Catal Lett 133:307–313
37. Wang LC, Huang XS, Liu Q, Liu YM, Cao Y, He HY, Fan KN, Zhuang JH (2008) J Catal 259:66–74
38. Zhang J, Su DS, Zhang AH, Wang D, Schlögl R, Hebert C (2007) Angew Chem Int Ed Engl 46:7319–7323
39. Veith GM, Lupini AR, Rashkeev S, Pennycook SJ, Mullins DR, Schwartz V, Bridges CA, Dudney NJ (2009) J Catal 262:92–101
40. Abid M, Paul-Boncour V, Touroude R (2006) Appl Catal A Gen 297:48–59
41. Tsubaki N, Fujimoto K (2003) Top Catal 22:325–335
42. Ilieva L, Pantaleo G, Ivanov I, Nedyalkova R, Venezia AM, Andreeva D (2008) Catal Today 139:168–173
43. Ilieva L, Pantaleo G, Nedyalkova R, Sobczak JW, Lisowski W, Kantcheva M, Venezia AM, Andreeva D (2009) Appl Catal B Environ 90:286–294
44. Zhao MW, Shen MQ, Wang J (2007) J Catal 248:258–267
45. Leppelt R, Schumacher B, Plzak V, Kinne M, Behm RJ (2006) J Catal 244:137–152